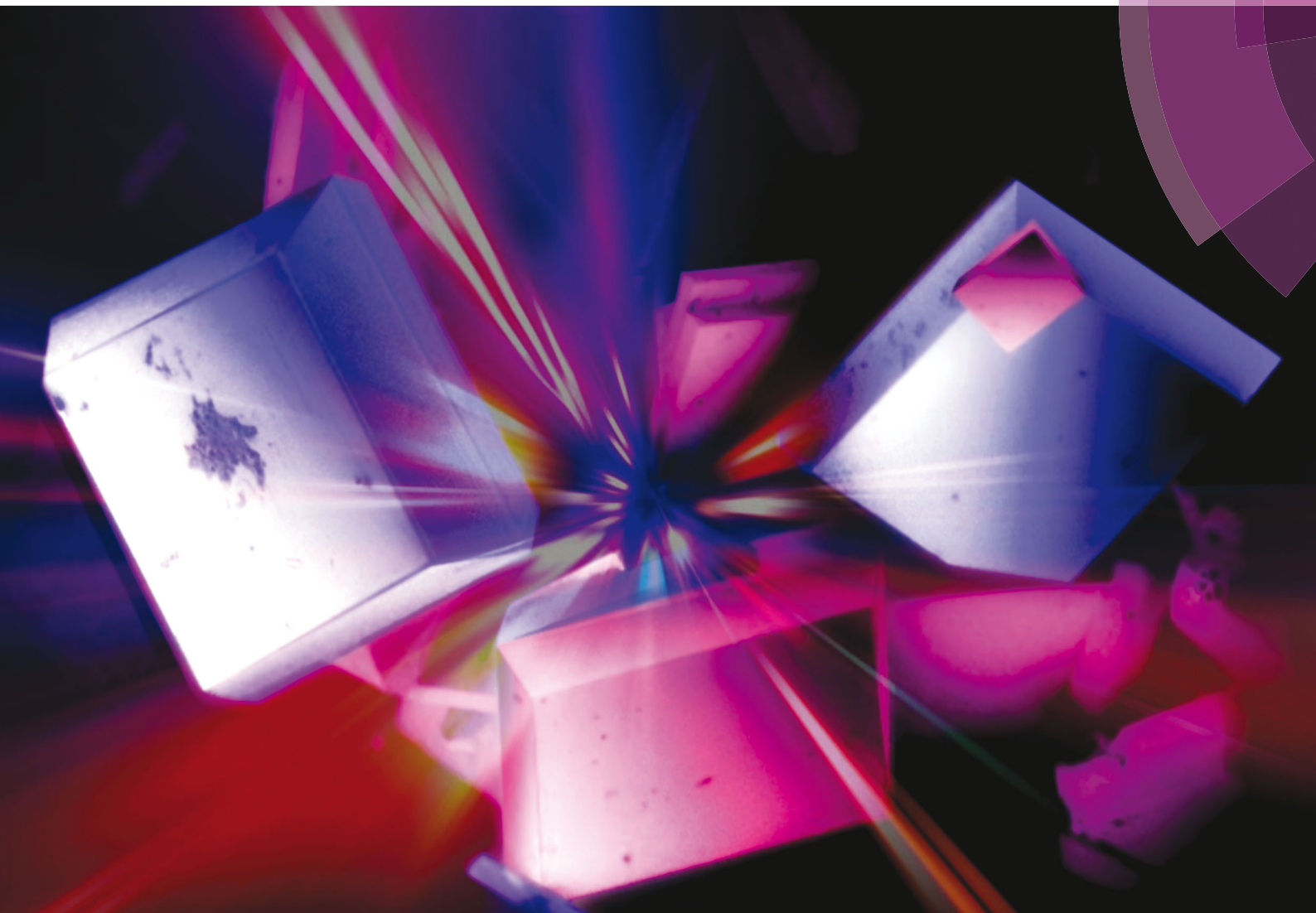


NJC

New Journal of Chemistry
rsc.li/njc

A journal for new directions in chemistry



Themed issue: Vanadium Science: Chemistry, Catalysis, Materials, Biological and Medicinal Studies

ISSN 1144-0546



ROYAL SOCIETY
OF CHEMISTRY

Celebrating
IYPT 2019

PAPER

Eglantina Benavente, Guillermo González *et al.*
Ammonium hexadeca-oxo-heptavanadate microsquares.
A new member in the family of the V_7O_{16} mixed-valence
nanostructures



Cite this: *New J. Chem.*, 2019, 43, 17548

Ammonium hexadeca-oxo-heptavanadate microsquares. A new member in the family of the V_7O_{16} mixed-valence nanostructures†

 Daniel Navas,^a José Pedro Donoso,^b Claudio Magon,^b Clivia M. Sotomayor-Torres,^{cd} Mabel Moreno,^{ef} Harold Lozano,^b Eglantina Benavente,^{ag} and Guillermo González^{bh}

This paper presents a new mixed valence heptavanadate $(NH_4)_2V_7O_{16}$, obtained from a two-stage treatment in a single container of ammonium metavanadate with hexadecylamine in an acetic medium. The hydrolysis of the precursor under normal conditions leads to an intermediate, layered hybrid nanocomposite, V_2O_5 /alkylamine, which after an *in situ* hydrothermal treatment is transformed almost quantitatively into an amine-free microcrystalline phase constituted by perfect square microparticles of $(NH_4)_2V_7O_{16}$. The analysis of composition, structure and morphology of the product points to a mixed valence vanadium oxide with a high content of V(IV) (approximately 73%). The microsquares have a tetragonal structure similar to that of BaV_7O_{16} , as well as to those proposed for the VO_x /amine hybrid nanocomposite series: nanotubes, nano urchins and the compound $(en)V_7O_{16}$. The results suggest that all these phases belong to the V_7O_{16} family, but that they differ in the amine content, the degree of reduction and the curvature of the network. The feasibility of obtaining flat nanostructures based on V_7O_{16} without templates, beyond demonstrating the robustness of the structural unit V_7O_{16} in networks with different degrees of reduction and curvatures, clarifies the role of alkylamines in this type of anti-entropic supramolecular process. First, the amine provides a stable platform that allows for an orderly reduction of the network under hydrothermal conditions and, when the medium favours the stability of the V–amine bond, the alkylamine contributes to the driving force that leads to the curving of the V–O network.

Received 29th April 2019,
Accepted 19th June 2019

DOI: 10.1039/c9nj02188d

rsc.li/njc

Introduction

Vanadium oxide-based compounds have received a great deal of attention because of their special physical and chemical

properties and ensuing potential applications.¹ The often colourful appearance of vanadium species—the origin of the element name (Vanadis, Scandinavian Goddess of Beauty)—denotes a challenging rich redox and coordination chemistry,² useful for developing materials sensitive to low-energy stimuli which are important for applications, for instance, in chemical and biochemical catalysis, energy storage or sensor devices. Vanadium is a widely distributed element in the biosphere, which as a heavy metal is in general considered a harmful pollutant, particularly when there is vanadium(V).³ However, at trace levels, vanadium has proven to be essential for some living organisms.⁴ The development of knowledge about oxidation states, redox chemistry and coordination of vanadium species associated with their biological role in enzymes such as some peroxidases or nitrogenases ones constitutes an important topic of modern bio-inorganic chemistry. Due to the recognised therapeutic effects of some vanadium-based formulations that mimic the action of insulin in mammals and their possible effect to treat some types of cancer,⁵ the interest in this chemistry has increased markedly. Vanadium multivalence is also very useful in homogeneous chemical catalysis.

^a Universidad Tecnológica Metropolitana, Departamento de Química, P. O. Box 9845, Santiago, Chile. E-mail: ebenaven@utem.cl

^b IFSC, Universidade de São Paulo, P. O. Box 369, 13560-970 São Carlos, SP, Brazil

^c Catalan Institute of Nanoscience and Nanotechnology (ICN2), CSIC and BIST, Campus UAB Bellaterra, 08193 Barcelona, Spain

^d ICREA, Pg. Lluís Companys 23, 08010 Barcelona, Spain

^e Max Planck Institute of Microstructure Physics, Weinberg 2, 06120, Halle, Germany

^f Universidad SEK, Instituto de Investigación Interdisciplinar en Ciencias Biomédicas SEK (I3CBSEK), Facultad Ciencias de la Salud, Fernando Manterola 0789, Providencia, Santiago, Chile

^g Programa Institucional de Fomento a la I + D + i, Universidad Tecnológica Metropolitana, Ignacio Valdivieso 2409, P. O. Box 8940577, San Joaquín, Santiago, Chile

^h Universidad de Chile, Departamento de Química, P. O. Box 653, Santiago, Chile. E-mail: ggonzale@uchile.cl

† Electronic supplementary information (ESI) available. See DOI: 10.1039/c9nj02188d

For example, in the oxidation of organic compounds with peroxides, H_2O_2 or oxygen assisted by vanadium compounds.⁶ Interestingly, this same type of reaction could be used to remediate contaminated soils by reducing the relative concentration of vanadium(v) performing a Felton-like heterogeneous catalytic process *in situ*.⁷ Recently, laminar hybrid nanocomposites based on vanadium oxide have also been shown to be effective as co-catalysts in heterojunctions with ZnO/fatty-acid hybrids for the photodegradation of dyes in aqueous systems with visible light.⁸

The vanadium oxide materials have demonstrated promising performance as materials for lithium-,⁹ sodium-¹⁰ or potassium-ion batteries.¹¹ However, the efficiency of these systems depends on the stability of the host vanadium oxide network. A robust network capable of accommodating lithium ions without severely altering its structure prevents the segregation of phases that would affect the transport of mass and charge on the electrode.¹² Vanadium oxide based layered nanostructures with various vanadium oxidation states are also studied as gas sensor materials.^{13,14}

Among the vanadium derivatives of mixed valence are the hybrid tubular nanostructures of vanadium oxides with alkylamines, particularly the nanotubes (VO_xNTs) and nano-urchins (NUs), in which the average oxidation state of vanadium is around +4.42 and +4.38, respectively.¹⁵ The VO_xNTs synthesised for the first time by the Nesper group are open tubes with walls in the range of 5–10 nm thick, formed by approximately 5–6 concentric layers of oxide interspersed with long-chain monoalkylamines.¹⁶ The NUs synthesised for the first time by our laboratory are three-dimensional micrometric particles (9–12 μm in diameter) formed by highly dense VO_xNT spherical matrices.¹⁷ The preparation strategies of both VO_xNTs and NUs are similar; essentially through the hydrothermal treatment of a flat laminar precursor which can be described as the intercalation of the corresponding amine in the vanadium(v) oxide hydrogel (V_2O_5). In fact, this intercalation is carried out by a supramolecular process based on the sol-gel condensation of the oxide on a double layer of surfactant (amine) that acts as a two-dimensional (2D) template. Virtually any precursor of V_2O_5 hydrogel can be used as a source of vanadium.¹⁸ The hydrothermal treatment (6–8 days at 180 °C) of the lamellar solid leads, almost quantitatively, to practically pure tubular products, provided that the carbon chain of amine C_n is in the range ($\text{C}_n\text{H}_{2n+1}\text{NH}_2$ with $4 \leq n \leq 22$). VO_xNTs may also be produced using diamines ($\text{H}_2\text{N}[\text{CH}_2]_n\text{NH}_2$ with $4 \leq n \leq 22$).¹⁹ At the same time, vanadium(v) is partially reduced to vanadium(IV). However, according to Vera-Robles *et al.*,¹⁸ the generation of VO_xNTs can also be achieved with excellent yields by chemical oxidation of a vanadium precursor in a lower oxidation state but provided an amphiphilic amine is present. Vanadium oxide nanotubes with mixed valence $\text{V}^{5+}/\text{V}^{4+}$ are structurally very stable species, capable of maintaining their tubular structure even after exchanging their original organic component with other low molecular weight amines, including ammonia, or with a variety of inorganic cations.^{20–22} Regardless of the oxidation state of vanadium in VO_xNTs or NUs, the

structural unit in these nanostructures appears to be the same, which is also very similar to that determined by Wang *et al.*²³ by the XRD single crystal analysis of the compound $\text{BaV}_7\text{O}_{16}$, prepared in a small amount from metallic vanadium by electrochemical-hydrothermal synthesis. The $\text{BaV}_7\text{O}_{16}$ has a laminar structure where each sheet is a flat polyanionic species constructed by condensation of the $\text{V}_7\text{O}_{16}^{2-}$ units. In bulk, these sheets are stacked in a direction normal to the molecular plane with Ba^{2+} counterions located in the interlaminal space. Each molecular unit $\text{V}_7\text{O}_{16}^{2-}$ is formed in turn by two layers, each of three distorted VO_6 octahedrons oriented in the opposite direction, which are joined together by a tetrahedral VO_4 unit.

Although the morphological analysis of the VO_xNT and the NU clearly shows that the tubes are generated by a rolling process,²⁴ in our opinion there are still open questions about the driving force and the mechanism of the process. Considering the rich diversity of coordination and the versatile redox chemistry typical of vanadium oxides, it is difficult to understand the generation of morphologically pure mixed valence phases such as VO_xNTs and NUs under hydrothermal conditions. Undoubtedly, as has been repeatedly argued in the literature,^{25,26} an important factor is the change in the oxidation state of vanadium produced by reaction with electron donors such as water or amines at hydrothermal temperatures. However, the role of amphiphiles like long chain amines in the process has been little discussed. In this sense, the reports by both Rappolo and Worle are interesting.^{15,20} These authors reported that the same VO_xNT synthesis strategy but using ethylenediamine instead of long carbon chain amines as a template, leads to a laminar product structurally similar to VO_xNTs and NUs, but with an almost flat open morphology, with just a small curvature. The elementary cell of the product is qualitatively similar to those of VO_xNTs and NUs, differing significantly only on the *c* axis.

In this paper, we report the preparation of a new carbonless member of the VO_xNT and NU families, the ammonium hexadeca-oxo-heptavanadate $(\text{NH}_4)_2\text{V}_7\text{O}_{16}$, where ammonium ions replace the long carbon chain amines. The tetragonal symmetry of the crystalline structure of the product, very similar to that of its homologue $\text{BaV}_7\text{O}_{16}$, is reflected in its almost perfect square-planar morphology. The preparation strategy and properties of $(\text{NH}_4)_2\text{V}_7\text{O}_{16}$ corroborate the structural stability of this family of vanadium oxides in a wide range of oxidation states. In addition, the results help to understand the role of amine amphiphiles in both the coiling mechanism and the supramolecular nature of the redox process underlying the formation of this class of mixed valence vanadium oxides.

Experimental section

Materials and methods

All chemical reagents used in the experiments were obtained from commercial sources as guaranteed grade reagents

purchased from Aldrich. All reagents were of analytical grade and were used without further purification.

Synthesis

NH_4VO_3 puriss $\geq 99\%$ (0.236 g, 3 mmol) and 1-hexadecylamine (HDA) puriss $\geq 90\%$ (0.268 g, 1 mmol) are mixed with 10 mL of absolute ethanol in a 100 mL flask. After 2 hours of vigorous stirring, 5 mL of glacial acetic acid is added. The yellow suspension is stirred for 30 minutes and 10 mL of double distilled water is added. An orange composite is formed and is stirred for 48 hours. This suspension is aged for 5 days. The hydrothermal treatment is performed in a Teflon-lined Parr Bomb at 180 °C, at differing durations of 24 hours, 3 days, 7 days and 10 days. The resulting black solid is washed several times with ethanol and dried under active vacuum at 80 °C. The amount of resulting black solid was 0.150 g, yield above 80%.

The chemical composition obtained from elemental analysis (%) for the products is found to be, for the intercalation compound, experimental (calculated for $\text{V}_2\text{O}_5(\text{HDA})_{1.0} \cdot 2.3\text{H}_2\text{O}$ with 3.07% VO_2): C 40.03 (39.99), N 2.99 (2.99), H 8.46 (8.46); and for the microsquares, experimental (calculated for $(\text{NH}_4)_2\text{V}_7\text{O}_{16}$ with 1.38% $\text{V}_2\text{O}_5/\text{HDA}$ and 6.48% VO_2): C 0.65 (0.63), N 4.02 (4.02), H 1.25 (1.25).

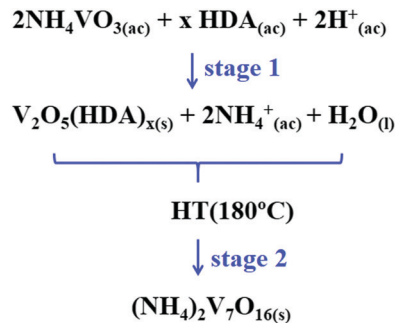
The content of vanadium(IV) in the products determined by colorimetric titration of the samples with KMnO_4 ¹⁵ is found to be, for the intercalation compound, $4.2 \pm 0.3\%$ and for the microsquares, $73.3 \pm 0.2\%$. Experimental details of the titration are presented in the ESI.†

Characterisation methods

Structural studies. Information was obtained from Powder X-Ray Diffraction (XRD), transmission electron microscopy (TEM) and scanning electron microscopy (SEM). Room temperature XRD data were collected using a Siemens D5000 diffractometer (Cu $K\alpha$, $\lambda = 1.5418 \text{ \AA}$, Operation voltage 40 kV). Data were collected in a continuous manner with a speed of $0.50^\circ \text{ min}^{-1}$ over the range $1.7^\circ < 2\theta < 80^\circ$. The morphological characterisation of the products was performed by field emission scanning electron microscopy (FESEM) using a JEOL JSM-6700F field-emission scanning electron micrograph with a suitable resolution to study the external morphology. The scanning electron microscopy (SEM) images were obtained by using an EVO MA 10 ZEISS microscope. The samples were prepared by the drop casting suspension technique and placed on a holey carbon support. TEM and electron diffraction (ED) were conducted using a JEOL-2000FX operating at 200 kV. The chemical composition of the samples was determined by elemental chemical analysis using a SISON model EA-1108 analyser. The FT-IR spectra were recorded using the KBr technique in a PerkinElmer series 2000 apparatus in the $4000\text{--}450 \text{ cm}^{-1}$ region.

Results

The preparation of $(\text{NH}_4)_2\text{V}_7\text{O}_{16}$ microsquares is a one-pot process, which, however, involves two well-defined consecutive stages (Scheme 1).



Scheme 1 Synthesis of $(\text{NH}_4)_2\text{V}_7\text{O}_{16}$.

The first stage corresponds to the hydrolysis at room temperature of the vanadium precursor NH_4VO_3 in aqueous amine solution, acidified after approximately two hours with acetic acid, which leads to a suspension of an orange solid. The interruption of the reaction at this point allows the orange intermediate to be denoted as a vanadium(v)/amine laminar nanocomposite similar to those previously detected in the preparation of VO_xNTs and NUs .¹⁷ The second reaction stage consists of the hydrothermal treatment of the previous orange suspension, which—on acquiring a black colour—points to the reduction of V(v) to (iv). In addition, no nanotube formation was detected, and the main product was identified as the amine-free ammonium vanadate $(\text{NH}_4)_2\text{V}_7\text{O}_{16}$ (Scheme 1). This new product has a lamellar nature, but instead of the typical appearance of nanocomposites of vanadium oxide, it exhibits a disordered superposition of extended leaves, consisting of a phase constituted by crystalline particles that are almost perfectly square and flat.

The chemical analysis of the orange solid obtained in the first reaction stage shows a high content of carbon and hydrogen (40.0 and 8.5%, respectively) and a small amount of vanadium(IV). Analysis fits the stoichiometry of $\text{V}_2\text{O}_5(\text{HDA})_{1.0} \cdot 2.3\text{H}_2\text{O}$ with an impurity equivalent to about 3.1% VO_2 , which approximately agrees with the content of V(IV) determined experimentally (*ca.* 4.2%). The presence of a small amount of V(IV) in the product is consistent with the ESR studies of xerogel V_2O_5 reported in the literature.^{27,28} The diffraction pattern of the product (Fig. 1a) dominated by the reflections of Bragg $00l$ ($l = 1$ to 3) corresponds to a laminar nanocomposite with an interlaminal space of approximately 2.68 nm. It is assumed

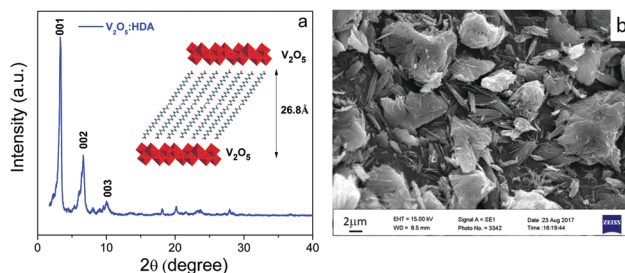


Fig. 1 Laminar nanocomposite $\text{V}_2\text{O}_5/\text{HDA}$ (a). X-ray diffraction (XRD) and structural model (insert); scanning electron microscopy (SEM) image (b).

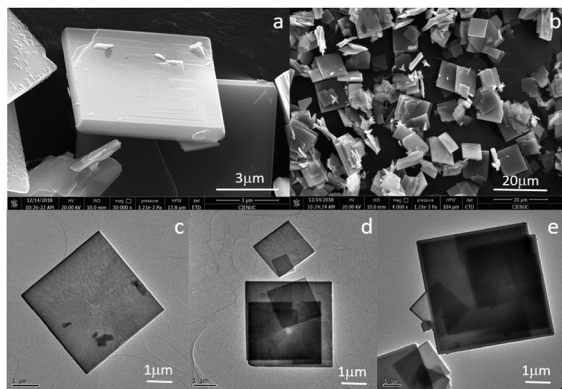


Fig. 2 $(\text{NH}_4)_2\text{V}_7\text{O}_{16}$ microsquares morphology: (a) and (b) SEM images; (c)–(e) transition electron microscopy (TEM) images.

that the amine is located in the interlamellar space with its polar heads oriented towards the vanadium–oxygen sheets with their hydrocarbon chains self-assembled in an interdigitated manner with an inclination of 37° to optimise the van der Waals interactions between the carbon chains²⁹ (model inserted in Fig. 1a). In Fig. 1b, the image SEM shows the layered nature with multi-layer plates.

Fig. 2(a) and (b) illustrate SEM micrographs of a typical sample of black microcrystalline solids obtained from a hydrothermal reaction (stage 2). The obtained phase is practically constituted only by well-formed square microcrystals with lateral sizes ranging from 1.8 to 4.4 μm and widths between 200 and 500 nm. The images of the surface of the crystals reveal characteristics that indicate that these squares are of a laminar nature and that they correspond to the stacking of nanometric sheets, practically all with 2D aspect ratios close to one.

The TEM images reproduced in Fig. 2(c) and (d) corroborate the almost completely symmetrical shape of the crystals. The presence of the ultrathin films points to an exfoliation of the crystals produced by the preparation of the samples. The composition of the product calculated from the elemental analysis and the redox titration corresponds to the compound $(\text{NH}_4)_2\text{V}_7\text{O}_{16}$, contaminated by a small amount of unreacted precursor nanocomposite (approximately 1.3% w/w) and an excess of V(IV) equivalent to *ca.* 6.5% of VO_2 .

To corroborate the mixed valence state of the $(\text{NH}_4)_2\text{V}_7\text{O}_{16}$ microsquares, we performed the X-ray Photoelectron Spectroscopy (XPS) study illustrated in Fig. 3. We used the oxygen vanadyl peak O1s energy level, at 530.0 eV, as reference bonding energy (BE) as well as to compensate charge and to determine the Shirley background underneath the V2p region. The long scan spectrum (Fig. 3a) shows the composition of the sample where the absence of the important contribution of possible impurities is apparent. Fig. 3b illustrates the high resolution XPS spectrum in the V2p states region where we observe the typical two peaks structure of V2p, due to spin–orbit splitting, and the single O1s peak from the oxygen atoms bonded to the vanadium atoms.^{30,31} To estimate the valence state composition of the sample, we analysed the relative peak area ratio of V2p to O1s. Consequently, we simulated the spectrum with mixed Lorentzian–Gaussian functions

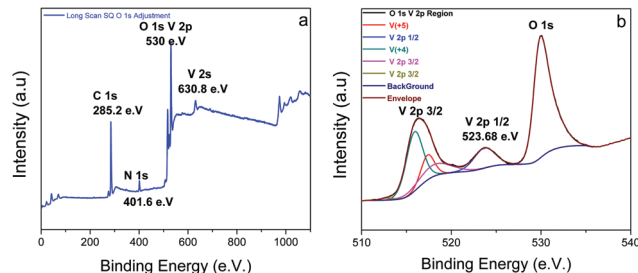


Fig. 3 X-ray photoelectron spectrum (XPS) of $(\text{NH}_4)_2\text{V}_7\text{O}_{16}$: (a) long-scan spectrum; (b) high-resolution XPS of the V2p and O1s state region.

(Voigt functions, CASA software) taking particularly into account the element photoionisation cross sections and the BE difference as well as the intensity ratio of the peaks $\text{V}2\text{p}_{3/2}$ and $\text{V}2\text{p}_{1/2}$ of 7.4 eV and 2 : 1, respectively. Results are shown in Fig. 3b and Table S1 (ESI[†]). From fitted components of the peak $\text{V}2\text{p}_{3/2}$ corresponding to both the V^{4+} and V^{5+} ions, centred at 515.88 eV and 517.33 eV, respectively, the average surface formal oxidation state of vanadium in $(\text{NH}_4)_2\text{V}_7\text{O}_{16}$ was found to be 4.25. Within experimental errors, this value agrees reasonably with both values, that measured by redox titration (4.27) and that calculated from the stoichiometry of the compound (4.29) (Table S1, ESI[†]).

To further investigate the chemical nature of $(\text{NH}_4)_2\text{V}_7\text{O}_{16}$, we analysed the molecular structure of microsquares using Fourier transform infrared spectroscopy (FTIR). In Fig. 4 we compared the FTIR spectra of $(\text{NH}_4)_2\text{V}_7\text{O}_{16}$ with that of the laminar intermediate V_2O_5 –amine detected in its preparation. In the nanocomposite (Fig. 4a), the vibrational signatures of hexadecylamine and vanadium oxide are clearly detected. We observe the asymmetric stretching and bending vibration modes of the NH_2 group at 3203 and 1514 cm^{-1} , respectively. Meanwhile, the vibrations $\nu_s(\text{CH}_2)$ and $\nu_{\text{as}}(\text{CH}_2)$ appear at 2848 and 2920 cm^{-1} , respectively. On the other hand, we

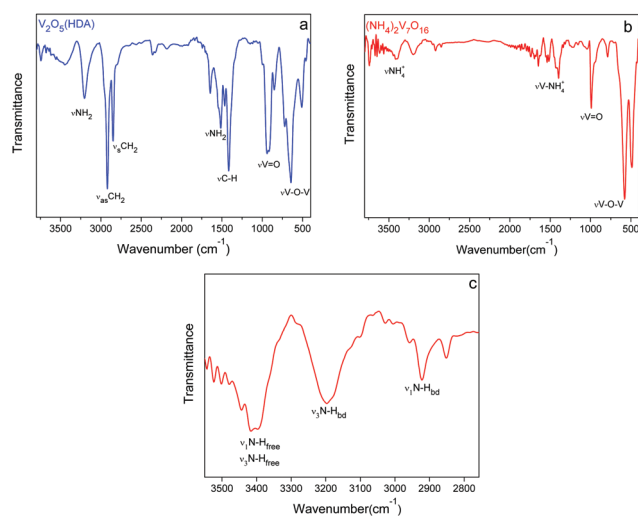


Fig. 4 Fourier transform infrared spectroscopy (FTIR) spectra of the V_2O_5 /HDA nanocomposite (a), $(\text{NH}_4)_2\text{V}_7\text{O}_{16}$ microsquares (b), and $(\text{NH}_4)_2\text{V}_7\text{O}_{16}$ N–H stretching vibration modes (c).

observe the absorptions associated with the V_2O_5 network in the region $1000\text{--}480\text{ cm}^{-1}$: the VOV stretch mode (bridged oxygen) at 721 cm^{-1} ; the mode of stretching of the group with tri-coordinated oxygen, at 644 cm^{-1} ; and the combination of stretching and bending modes of groups with a triple-coordinated oxygen at 511 cm^{-1} . In the spectrum of the microsquares, there is only one absorption band assignable to the mode of stretching vanadyl bonds, a sharp peak at a relatively low frequency, 941 cm^{-1} .^{32,33} This is interesting because it is a frequency that corresponds to a high content of V(IV) in the compound and also because this band shape would reflect that there is only one type of atom of V. The atoms V(IV) and V(V) are indistinguishable under conditions of measurement, pointing to a charge delocalization, characteristic of mixed valence structures. A further description of the IR spectrum of the products and their comparison with the VO_xNT spectrum,³³ in the characteristic frequency range of the oxovanadates, is shown as additional information (Table S3, ESI†). The spectrum of $(NH_4)_2V_7O_{16}$ (Fig. 4b) differs from that of the nanocomposite, particularly in the spectral region around 3500 and 1350 cm^{-1} . The characteristic absorptions of hexadecylamine are practically absent, but instead, there are features assignable to the N–H vibration of the ammonium ion, both free and with hydrogen bonds to the vanadium oxide matrix. We suggest that the band centred at 3426 cm^{-1} comprises the asymmetrical and symmetric stretching vibrations of the free N–H bonds, while those centred at 3196 and 2922 cm^{-1} belong to the asymmetric and symmetric stretching modes of the NH bonds coupled to the matrix, respectively (Table S2, ESI†). It is also worth mentioning the reduced symmetry of the NH_4^+ ion in $(NH_4)_2V_7O_{16}$ (from t_d to C_{2v}), which allows the detection of its four fundamental modes of vibration by infrared solid spectroscopy (KBr). In addition, the coexistence of free N–H bonds and H bonds observed at frequencies similar to those registered in the gas phase systems reflects the nature of the interlaminal phase in this compound.³⁴

Fig. 5 shows the typical XRD pattern of the microsquares $(NH_4)_2V_7O_{16}$ characterised mainly by a sequence of relatively

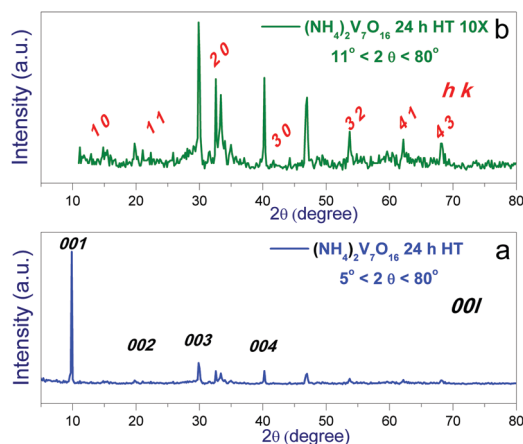


Fig. 5 XRD pattern of the $(NH_4)_2V_7O_{16}$ microsquares (a); part of the same amplified by 10 (b).

narrow equidistant Bragg peaks that point to the presence of layered microcrystals with preferential orientation. The interlaminal space d determined from the complete set of diffractograms is 0.89 nm . This basal separation is similar to that observed in other intercalated ammonium ions: for example, 0.90 nm in the NH_4^+ /amine VO_xNTs ,³⁵ 0.94 nm in $(NH_4)_{0.5}V_2O_5 \cdot mH_2O$,³⁶ or NH_4^+ in interleaf xerogels,³⁷ as well as the separation in the intercalation of metal ions, such as Na^+ and Ca^{2+} in VO_xNTs with the interlaminal distances of 0.90 nm ³⁸ and approximately $0.90\text{--}1.10\text{ nm}$,²² respectively. The indexing of the XRD pattern of the nanosquares consigned in Fig. 5(a) and $10\times$ in Fig. 5(b), including the planes of the Bragg reflections series $(00l)$ and $(hk0)$, corresponds to a two-dimensional tetragonal network with a basal distance, a , of 6.1 (Fig. S1, ESI†). The reflection peaks $(hk0)$ have an approximately Lorentzian shape; however, they generally show an asymmetrical sawtooth profile that suggests a turbostratic disorder between the layers.³⁹ In fact, no (khl) reflection is detected. The DRX pattern of $(NH_4)_2V_7O_{16}$ XRD qualitatively coincides with those observed in VO_xNTs ¹⁹ and NUs ¹⁷ as well as in $(en)_2V_7O_{16}$,²⁰ where the reflections $(hk0)$ seem to be insensitive to the type of intercalated host.

The typical selected area electron diffraction (SAED) pattern of the microsquares illustrated in Fig. 6 suggests a tetragonal network with $a = 0.615\text{ nm}$ agreeing with the XRD results. Consequently, the crystal structure we propose for $(NH_4)_2V_7O_{16}$ is similar to that of BaV_7O_{16} —a tetragonal network with $a \sim 0.617\text{ nm}$ —²³ and only slightly different from those reported for the VO_xNTs : lattice networks with $a = 0.61$,²² 0.615 ,⁴⁰ or 0.62 nm ,¹⁸ as well as that of the triclinic network $(en)V_7O_{16}$ with $a = 0.616$ and $b = 0.617$.^{15,20}

In the structure of the anion $V_7O_{16}^{2-}$, the VO_6 units are distorted octahedra with the axial V–O bond opposite to the vanadyl group $V=O$ significantly weaker than the equatorial ones (Fig. 7a) Therefore, the structure of $V_7O_{16}^{2-}$ can be seen, as shown in Fig. 7b. This is like a complex polyanionic flat sheet neutralized by NH_4^+ ions distributed on the surface. In turn, each sheet is formed by two parallel layers of square-pyramidal polyhedrons, oriented in the opposite direction with respect to the $V=O$ bond, joined together by tetrahedral VO_4 units separated periodically. Therefore, bulk square microcrystals would be stacked $(V_7O_6)_n^{2n-}$ sheets interspersed with NH_4^+ ions (Fig. 7b). This description agrees with the intensities pattern of the harmonics $(00l)$ —odd—even—observed in the diffractogram (Fig. 5a). This phenomenon, where the intensities of the even-order reflections—especially the (002) ones—appear

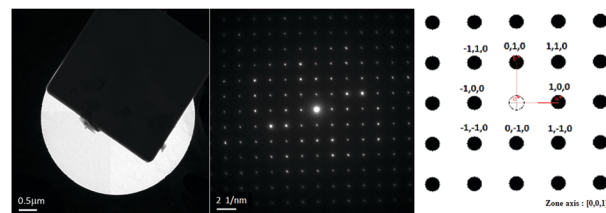


Fig. 6 Selected area electron diffraction (SAED) pattern of a microcrystal of $(NH_4)_2V_7O_{16}$.

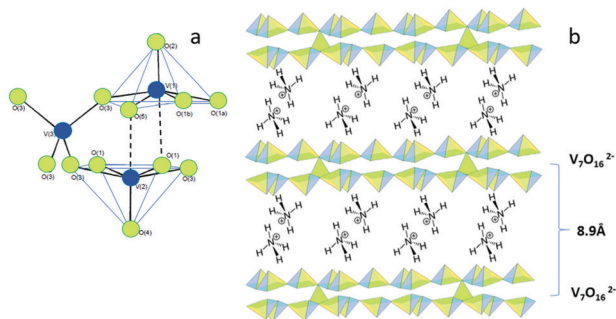


Fig. 7 Structural model of $(\text{NH}_4)_2\text{V}_7\text{O}_{16}$, adapted from the structure of $\text{BaV}_7\text{O}_{16}$ reported by Wang *et al.*²² (a) Model of the anionic cluster $(\text{V}_7\text{O}_{16})^{2-}$; (b) model of stacked bilayers for the bulk product.

markedly depressed, is similar, for example, to the stacking of the double layers in ribbons and sheets of $\text{V}_2\text{O}_5 \cdot n\text{H}_2\text{O}$ gels modeled by Oka *et al.*,⁴¹ or as observed for the partially reduced V_2O_5 , $(\text{NH}_4)_{0.5}(\text{V}_2\text{O}_5)$.⁴² As far as we know, such an X-ray interference pattern has never been observed in the nanostructures V_7O_{16} , VO_xNTs or NUs , probably due to poor coherence between the plates because of their curvature.

The crystal structure of $(\text{NH}_4)_2\text{V}_7\text{O}_{16}$ appears to be thermally quite stable under hydrothermal conditions. Indeed, as observed in Fig. S2 (ESI[†]), the products obtained from a series of experiments performed using thermal treatments of different durations, from 0.5 to 7 days, show practically the same DRX pattern. However, after thermal treatment for longer than seven days, they begin to decompose. Fig. 8 shows a typical SEM image of the product obtained after 10 days. The formation of a new rather homogenous vanadium oxide phase, mostly constituted by cross-shaped particles is evident. Although we have not yet studied this phase in detail, the preliminary characterisation showed that the micro crosses do not contain nitrogen and that in them vanadium oxidation is near to that of VO_2 . DRX analysis (Fig. S3, ESI[†]) shows a pattern that agrees with that of the phase $\text{V}_{0.87}\text{O}_2$ which is similar to our six-times rotationally symmetrical vanadium oxide-based nanostructures with a cog-like architecture⁴³ as well as to the hexangular starfruit-like VO_2 , reported more recently.⁴⁴

Our results agree with that reported in the literature concerning the importance of long-chain alkylamines in the hydrothermal synthesis of morphologically pure phases of mixed valence vanadium oxides.²⁵ The formation of micro-squares, as well as VO_x nanotubes, obtainable by reduction of

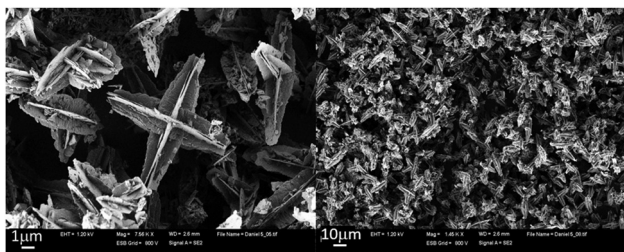


Fig. 8 Vanadium oxide micro crosses. SEM images of the product obtained after 10 days of hydrothermal treatment.

vanadium oxide(v) or by oxidation of vanadium(iv), is only achieved when an alkylamine is used as a template.

Discussion

The formation of nanotubes has been explained mainly in terms of the flexibility of the system associated with the partial reduction of vanadium. However, the results of this work encourage a somewhat more detailed analysis of the mechanistic aspects involved in these anti-entropic processes. In general, the formation of the different V_7O_{16} -based tubular nanostructures may be seen as the conjugation of two important processes, the partial reduction of vanadium and the curvature of the network. The conjugation of structural changes and redox processes promoted by hydrothermal conditions is not new in the chemistry of oxovanadates. An example of this is the influence of temperature and counterion on the synthesis and decomposition of sodium and tetramethylammonium decavanadate (TBA) salts as described, for example, by J. Livage's group.⁴⁵ Both salts can be precipitated from V_2O_5 solutions in the presence of NaOH or TBAOH at both alkaline and neutral pH. However, the thermal decomposition of these two solids leads to different products. $\text{NaV}_{10}\text{O}_{28}$ is decomposed in a mixture of sodium polyoxovanadate NaV_3O_8 and NaVO_3 , while that of TBA is partially reduced, transforming into laminar polyoxovanadate $\text{TMA}(\text{V}_4\text{O}_{10})$. These same polyoxometalates can also be obtained directly from V_2O_5 by hydrothermal treatment. In addition, the authors showed that these polymeric solids may also be precipitated from the respective decavanadate solutions previously pretreated at 200 °C (hydrothermal conditions). This is despite the fact that an ^{51}V NMR study showed that both solutions contained only vanadium(v). This suggests that the reduction stage induced by the presence of the organic cation would occur together with the precipitation of the species in solution. Apparently, a template effect similar to that leading to the transformation of V_2O_5 into mixed valence species V_7O_{16} would occur.

The first stage in the synthesis of V_3O_{17} species (Scheme 1) always corresponds to the formation of a laminar nanocomposite, stabilised by the two dimensional self-assembly of the surfactant and interaction of its head with the vanadium oxide. The vanadium structure in these nanocomposites is like that of their hydrogel,⁴⁶ where water can easily be replaced by amine in the space of the intermediate layer due to the relatively high Lewis-base activity of the latter. In contrast to the ligand exchange nature of the previous step, the second is characterized by the partial reduction of vanadium in the compound.

The vanadium oxide reduction process promoted by the hydrothermal conditions leading to these compounds appears to be an orderly process that is only possible if it occurs on the surface of a template stable enough to allow concomitantly both vanadium reduction and bond rearrangements involved in the transformation of V_2O_5 into V_7O_{16} units. An example of processes in which the template determines the structure of the products is the synthesis of perfectly ordered mesoporous silicates and aluminosilicates, known as MCM-41 based

materials. The use of long-chain tetraalkylammonium salts as templates, similar to the amines we use, makes it possible to generate hybrid sheets of two-dimensional hybrid silicates and convert them into tubular species by modulating the reaction conditions.⁴⁷

The long-chain monoalkylamines or diamines seem to be ideal for producing both processes. As far as we know, amines are the only amphiphiles able to produce this type of structure in such a successful way. Indeed, other types of surfactants such as alkyl thiols or polyethers are equally suitable for forming laminar species but fail to stabilise tubular hybrids or planar mixed-valence species as they do the amines. In these cases, the hydrothermal treatment produces a more enhanced reduction leading to template-free compounds with a mean vanadium oxidation state very close to 4+ that corresponds to Magnelli phases.⁴⁸ Interestingly, these products show characteristic morphologies with a hexagonal symmetry like, for example, the nanofruits⁴² or our nanocogs (Fig. S4, ESI[†]),⁴³ obtained using polyethers (Pluronic[®]) or alkyl thiols as templates, respectively.

Although other surfactants such as alkyl thiols can form bilayers as strong as amines, in the latter their self-assembly capability is combined with their peculiar coordinating ability derived from the electronic structure of the nitrogen atom, a typical monofunctional σ -donor. This contrasts with surfactants with donor atoms such as oxygen or sulphur which, because they also are π -donors, generate a smaller ligand field. Thus, it is expected that in the intercalation compounds the amine nitrogen atoms are relatively strongly coordinated to vanadium, especially at relatively high pH values.

The role of the coordination of alkylamine in the promotion of the partial reduction of V_2O_5 seems to arise from the modification of the electronic structure of the oxide. The structure of V_2O_5 in the hydrogel can be roughly described as a condensation of the VO_5 units in which the vanadium acquires a distorted octahedral configuration by coordinating a water molecule. In this context, the frontier orbitals in V_2O_5 and oxovanadates, HOMO and LUMO, would have mainly the character of oxygen-p and vanadium- t_{2g} , respectively. Due to the interaction with the oxygen-filled π -orbitals, the t_{2g} orbitals are antibonding. Therefore, by substituting the water molecules by purely Sigma ligands, such as amines, the t_{2g} orbitals will become partially nonbonded, the LUMO energy will be lower and the vanadium reduction will be energetically more suitable.

Comparing the average oxidation state of vanadium in the microsquares described here with those in the VO_x NTs and NUs seems to indicate that the degree of reduction of vanadium is related to the morphology of the products. Given the fact that the greater the planarity of the structure, the greater the degree of reduction, it is quite reasonable if we consider that planarity favours the delocalisation of electrons in the system.

The fact that the same type of intermediary, the nano-composite V_2O_5 /alkylamine, generates in one case organic-inorganic hybrid nanotubes and in the other one, purely inorganic microsquares is due only to a subtle difference in the reaction conditions; namely, the addition of acetic acid to

the reaction medium in the case of microsquares. Although the increase in acidity of the medium does not prevent the formation of the intermediate nanocomposite under normal reaction conditions, it is enough to induce the segregation and replacement of the amine under hydrothermal conditions. This is possibly mainly due to the destabilisation of the vanadium–nitrogen interaction by the protonation of the amine.

With respect to the reduction procedures, our experiments, or many others previously described in the literature cited above, have not allowed it to be determined whether the vanadium-reducing electron donor agent is the amine, the water, or both. However, we now believe that the reduction of vanadium(v) to vanadium(iv) must occur while the oxide structure is supported by the amine template. In the case of nanotubes where the amine remains attached to the inorganic structure, the reduction and rolling up processes are probably concomitant. Therefore, it is expected that the amount of charge transferred to the vanadium oxide structure is exactly that necessary to achieve the minimum energy determined by the curvature of the network. On the other hand, in the case of microsquares, both oxide reduction and amine/ammonium exchange must also occur concomitantly, until the minimum energy of the V_7O_{16} flat network is reached.

Considering that a flat V_7O_{16} structure is as or more stable than that of the nanotubes, it is necessary to explain why both types of compounds can be obtained independently as morphologically pure phases. The volume change of the VO_5 polyhedra associated with the reduction of vanadium(v) of certain atoms of the structure can lead to a curvature of the system.⁴⁹ However, it seems to us that that variable alone is not enough to justify such homogenous systems. We believe that the presence of the amine plays an important role in the formation of nanotubes.

As already mentioned above, at relatively high pH—like that used to obtain the nanotubes—the V–N bonds and the alkyl chain self-assembly do resist hydrothermal conditions. However, at high pressure and temperature, together with the change in water pK ($K_w \sim 10^{-12}$ at 180 °C and a self-generated pressure of approximately 10 bar), the diffusion of water into the interlaminar space is favoured which increases the degree of ionization and solvation of the amine group leading to a greater effective volume of the head of the surfactant. As schematically illustrated in Fig. S5 (ESI[†]), the characteristic cylindrical shape of the surfactant is transformed into a cone; in other words, there is a decrease in the so-called critical packaging parameter,⁵⁰ favouring the curvature of the template. In this way, this typical process of the supramolecular chemistry of the amphiphilic species would contribute to the necessary driving force for the rolling of the V_7O_{16} sheets.

Although our experiments contribute to the postulation of plausible mechanisms to explain the morphological richness and chemical versatility of the V_7O_{16} family, a deeper knowledge of these systems as well as the development of new applications, particularly in the field of catalysis, energy conversion and molecular magnetism, is still required. In this regard, spin resonance electronic studies are being conducted

to investigate the nature of the mixed valence of each member of the V_7O_{16} family.

Conclusions

The reaction of ammonium vanadate with hexadecylamine in an acetic medium leads to the formation of a new crystalline, vanadium oxide-based phase—the ammonium hexadeca-oxoheptavanadate, $(NH_4)_2V_7O_{16}$ —constituted almost entirely by highly symmetrical flat microsquares. This is a lamellar, mixed-valence vanadium compound where *ca.* 73% vanadium is formally in an oxidation state 4+. The synthesis strategy utilised, a two-step one-pot reaction, is similar to that used to synthesise VO_x NTs nanotubes and NUs where in the first stage a hybrid laminar nanocomposite, V_2O_5 /alkylamine intermediary can always be detected. However, during the hydrothermal treatment, the amine is segregated being replaced by ammonium ions, thus leading to a flat laminar surfactant-free structure.

The tetragonal structure of $(NH_4)_2V_7O_{16}$ is similar to that of BaV_7O_{16} as well as to that of the inorganic moiety in hybrid VO_x nanotubes, nanourchins and $(en)V_7O_{16}$. Therefore, the nano squares can be considered as a member of the same family of products, but with a flat laminar morphology, a higher vanadium(IV) content, and without the organic rest characteristic of its congeners. This confirms the robustness of the V_7O_{16} unit that remains intact in different networks with differences in reduction state and curvature.

The results obtained also allow us to better understand the role of long chain amines in the generation of the different phases based on V_7O_{16} . In the stage prior to the hydrothermal treatment, amine self-assembly generates a flat support on which the vanadium network may be reduced and reorganised under hydrothermal conditions, and, if the medium favours the stability of the V-amine bond, the alkylamine would contribute to the bending of the vanadium oxide sheet.

Finally, it is worth mentioning that the identification of the supramolecular processes, as well as the affinity of amine nitrogen for the vanadium centres detected, may be useful to rationalize many, current or future, studies and applications based on vanadium oxide chemistry.

Conflicts of interest

There are no conflicts to declare.

Acknowledgements

This work was supported by the Universidad de Chile, Universidad Tecnológica Metropolitana, FONDECYT 1171803, Fund of Scientific and Technological Equipment, 2018, L318-03 UTEM, CMST Spanish MINECO projects PHENTOM (FIS2015-70862-P) and Severo Ochoa (SEV-2013-0295) and the CERCA Programme/Generalitat de Catalunya and Conicyt-Programa Fondecip SEM EQM (150101).

References

- 1 A. Taroni, *Nat. Chem.*, 2017, **9**, 602.
- 2 P. Galloni, V. Conte and B. Floris, *Coord. Chem. Rev.*, 2015, **301–302**, 240–299.
- 3 G. Chen and H. Liu, *Environ. Sci. Technol.*, 2017, **51**, 11643–11651.
- 4 D. C. Crans, J. J. Smee, E. Gaidamauskas and L. Yang, *Chem. Rev.*, 2004, **104**, 849–902.
- 5 D. C. Crans, L. Yang, A. Haase and X. Yang, *Met. Ions Life Sci.*, 2018, **18**, 251–279.
- 6 D. S. Nesterov, O. V. Nesterova and A. J. L. Pombeiro, *Coord. Chem. Rev.*, 2018, **355**, 199–222.
- 7 G. Fang, Y. Deng, M. Huang, D. D. Dionysiou, C. Liu and D. Zhou, *Environ. Sci. Technol.*, 2018, **52**, 2178–2185.
- 8 J. Aliaga, N. Cifuentes, G. González, C. Sotomayor-Torres and E. Benavente, *Catalysts*, 2018, **8**, 374.
- 9 Y. Ma, A. Huang, H. Zhou, S. Ji, S. Zhang, R. Li, H. Yao, X. Cao and P. Jin, *J. Mater. Chem. A*, 2017, **5**, 6522–6531.
- 10 K. Zhang, G. Gao, W. Sun, X. Liang, Y. Liu and G. Wu, *RSC Adv.*, 2018, **8**, 22053–22061.
- 11 B. Tian, W. Tang, C. Su and Y. Li, *Reticular, ACS Appl. Mater. Interfaces*, 2018, **10**, 642–650.
- 12 G. A. Horrocks, Y. Luo, L. F. J. Piper, A. Parija, J. L. Andrews, L. R. De Jesus, J. Jude and S. Banerjee, *Chem. Mater.*, 2017, **29**, 10386–10397.
- 13 E. Strelcov, Y. Lilach and A. Kolmakov, *Nano Lett.*, 2009, **9**, 2322–2326.
- 14 J. Huotari, J. Lappalainen, J. Eriksson, R. Bjorklund, E. Heinonen, I. Minalainen, J. Puustinen and A. L. Spetz, *J. Alloys Compd.*, 2016, **675**, 433–440.
- 15 M. Roppolo, C. B. Jacobs, S. Upreti, N. A. Chernova and S. Whittingham, *J. Mater. Sci.*, 2008, **43**, 4742–4748.
- 16 M. E. Spahr, P. Bitterli, R. Nesper, M. Müller, F. Krumeich and H. U. Nissen, *Angew. Chem., Int. Ed.*, 1998, **37**, 1263–1265.
- 17 C. O'Dwyer, D. Navas, V. Lavayen, E. Benavente, M. A. Santa Ana, G. Gonzalez, S. B. Newcomb and C. M. Sotomayor Torres, *Chem. Mater.*, 2006, **18**, 3016–3022.
- 18 L. I. Vera-Robles and A. Campero, *J. Phys. Chem. C*, 2008, **112**, 19930–19933.
- 19 F. Krumeich, H. J. Muhr, M. Niederberger, F. Bieri, B. Schnyder and R. Nesper, *J. Am. Chem. Soc.*, 1999, **121**, 8324–8331.
- 20 M. Wörle, F. Krumeich, F. Bieri, H. J. Muhr and R. Nesper, *Z. Anorg. Allg. Chem.*, 2002, **628**, 2778–2784.
- 21 J. M. Reinoso, H. Muhr, F. Krumeich, F. Bieri and R. Nesper, *Helv. Chim. Acta*, 2000, **83**, 1724S.
- 22 S. Nordlinder, L. Nyholm, T. Gustafsson and K. Edstrom, *Chem. Mater.*, 2006, **18**, 495–503.
- 23 X. Wang, L. Liu, R. Bontchev and A. J. Jacobson, *Chem. Commun.*, 1998, 1009–1010.
- 24 X. Chen, X. Sun and Y. Li, *Inorg. Chem.*, 2002, **41**, 4524–4530.
- 25 J. Livage, *Materials*, 2010, **3**, 4175–4195.
- 26 Y. Wang and G. Cao, *Chem. Mater.*, 2006, **18**, 2787–2804.
- 27 P. Barboux, N. Baffier, R. Morine and J. Livage, *Solid State Ionics*, 1983, **9–10**, 1073–1080.

- 28 O. Nascimento, C. Magon, J. Lima and J. Donoso, *et al.*, *J. Sol-Gel Sci. Technol.*, 2008, **45**, 195–204.
- 29 L. Korosi, S. Papp and I. Dekany, *Chem. Mater.*, 2010, **15**, 4357–4363.
- 30 E. Hryha, E. Rutqvist and L. Nyborg, *Surf. Interface Anal.*, 2011, **44**, 1022–1025.
- 31 G. Silversmit, D. Depla, H. Poelman, G. B. Marin and R. De Gryse, *J. Electron Spectrosc. Relat. Phenom.*, 2004, **135**, 167–175.
- 32 C. O'Dwyer, V. Lavayen, D. Fuenzalida, H. Lozano, M. A. Santa Ana, E. Benavente, G. Gonzalez and C. M. Sotomayor-Torres, *Adv. Funct. Mater.*, 2009, **19**, 1–10.
- 33 W. Chen, L. Q. Mai, J. F. Peng, Q. Xu and Q. Y. Zhu, *J. Mater. Sci.*, 2004, **39**, 2625–2627.
- 34 K. Nakamoto, *Infrared Spectra of Inorganic and Coordination Compounds*, *Inorganic compounds II*, Wiley-Interscience, 1970, pp. 106–110.
- 35 K. S. Pillai, F. Krumeich, H. J. Muhr, M. Niederberger and R. Nesper, *Solid State Ionics*, 2001, **141–142**, 185–190.
- 36 G. T. Chandrappa, N. Steunou, S. Cassaignon, C. Bauvais and P. K. Biswas, *J. Sol-Gel Sci. Technol.*, 2003, **26**, 593–596.
- 37 P. Trikalitis, V. Petkov and M. G. Kanatzidis, *Chem. Mater.*, 2003, **15**, 3337–3342.
- 38 S. Nordlinder, A. Augustsson, T. Schmitt, J. Guo, L. C. Duda, J. Nordgren, T. Gustafsson and K. Edstrom, *Chem. Mater.*, 2003, **15**, 3227–3232.
- 39 C. O'Dwyer, V. Lavayen, D. Fuenzalida, H. Lozano, M. A. Santa Ana, E. Benavente, G. González and C. M. Sotomayor-Torres, *Small*, 2008, **7**, 990–1000.
- 40 W. Chen, J. Peng, L. Mai, Q. Zhu and Q. Xu, *Mater. Lett.*, 2004, **58**, 2275–2278.
- 41 T. Yao, Y. Oka and N. Yamamoto, *J. Mater. Chem.*, 1992, **3**, 331–336.
- 42 H. Wang, K. Huang, C. Huang, S. Liu, Y. Ren and X. Huang, *J. Power Sources*, 2011, **196**, 5645–5650.
- 43 C. O'Dwyer, V. Lavayen, D. Fuenzalida, S. Newcomb, M. A. Santa-Ana, E. Benavente and G. González, *Phys. Status Solidi B*, 2007, **244**, 4157–4160.
- 44 J. Shao, X. Li, Q. Qu and H. Zheng, *J. Power Sources*, 2012, **219**, 253–257.
- 45 L. Bouhedja, N. Steunou, J. Maquet and J. Livage, *J. Solid State Chem.*, 2001, **162**, 315–321.
- 46 J. Livage, *Coord. Chem. Rev.*, 1999, **190–192**, 391–403.
- 47 A. Monnier, F. Schuth, Q. Huo and D. Kumar, *et al.*, *Science*, 1993, **261**, 1299–1303.
- 48 H. Katzke, P. Toledano and W. Depmeier, *Phys. Rev. B: Condens. Matter Mater. Phys.*, 2003, **68**, 024109.
- 49 D. Mc Nulty, D. N. Buckley and C. O'Dwyer, *RSC Adv.*, 2016, **6**, 40932–40944.
- 50 S. Dutt, P. F. Siril and S. Remita, *RSC Adv.*, 2017, **7**, 5733–5750.